Machine Learning-Based Matching Medium Design for Implant Communications

E. Cil, C. Cadir, O.A. Kati, H. Birkan Yilmaz, S. Dumanli

This article has been accepted for publication in a future issue of this journal, but has not been fully edited. Content may change prior to final publication. Citation information: DOI 10.1109/TAP.2022.3140497, IEEE Transactions on Antennas and Propagation

Machine Learning-Based Matching Medium Design for Implant Communications

Erdem Cil, Cemre Cadir, Omer A. Kati, H. Birkan Yilmaz, *Member, IEEE*, and Sema Dumanli, *Member, IEEE*

***Abstract*—Matching media are used in various applications to increase the power transmitted into the human body. The selection of the optimum matching medium permittivity is not a straightforward task, as the optimum value maximizing the transmitted power depends on the thickness of the matching medium and the electromagnetic properties of the target tissue. In this paper, a computationally heavy empirical approach and a machine learning-based approach are utilized for the selection of the matching medium. The empirical approach demonstrates that the matching medium can increase the $|S_{21}|$ values up to 8 dB, which is validated with measurements. Next, a machine learning-based tool is proposed to predict the optimum matching medium permittivity for any target tissue and any matching medium thickness. A one-dimensional convolutional neural network followed by a multi-layer perceptron is trained with the simulated average Poynting vector magnitudes for muscle and fat as target tissues. The average Poynting vector magnitude and the dipole length for given system parameters are predicted by the trained artificial neural network. The accuracy is calculated by comparison with the results of the empirical analysis and found to be 1% and 12.3% mean absolute percentage error for dipole length and average Poynting vector magnitude, respectively. The proposed tool decreases the time required to milliseconds.**

***Index Terms*—Convolutional neural networks, implants, in-body link, machine learning.**

I. Introduction

In recent years, a continuously growing interest has been observed in the utilization of implantable devices in medical applications [1]. A great number of implantable devices have already been developed to be used in diverse medical applications such as health monitoring [2], [3] and medical treatment [4], [5] and the number of such devices is estimated to further increase in the coming years [6]. An implant may require establishing a wireless link with an on-body or an off-body device. This wireless link is commonly referred to as an in-body link [7]. It must be noted that establishing a reliable and high-quality in-body link is a challenging task.

The losses related to the in-body link can be classified into three categories: propagation losses, near-field losses and reflection losses at the air-human body boundary. The propagation loss is much higher for an in-body link compared to a link over the air due to the highly dissipative nature of human tissues, which can not be avoided [8]. On the other hand, near-field losses and reflection losses can be engineered. Near-field losses occur both in the implant and the wearable end of the in-body link due to lossy human tissues having conductivity (σ) [9], and the reflection losses are caused by the difference between the relative permittivities of air and human tissues [10]. When all these challenges are combined, they may lead to a significant deterioration of the in-body link.

The work presented in this paper focuses on the near-field and the reflection losses. Inserting a lossless controlled environment between the wearable antenna and the human body can help tackle these challenges. Such an environment is frequently referred to as the matching medium (MM) or the bolus layer [11]. Naturally, the optimum relative permittivity of an MM that ensures the highest reduction in reflection depends on various physical and electromagnetic (EM) properties of the specific case in which the medium is to be utilized. Particularly, parameters such as the thickness of the medium, the EM properties of the target tissue, hence the frequency, and the depth of the implant strongly affect the optimum value of the relative permittivity. Therefore, the selection of an MM for a specific case is a complicated problem and there is a lack of a well-established method in the current state of the art [12].

In the literature, there are many studies that make use of an MM without investigating whether the used value of relative permittivity is the optimum value that maximizes the power transmitted into the human body for the studied case [13]–[21]. As for the studies investigating the optimum relative permittivity for a specific case, the optimum relative permittivity is often determined for different tissue types via analytical studies or repeated numerical analyses. For instance, analytical studies that focus on the determination of the optimum relative permittivity for medical microwave applications are presented in [22]–[24]. However, all these studies assume the wave to be a plane wave, ignoring the near-field losses. In [25] and [26], a numeric human chest model embedded in an infinite MM is used along with a plane wave assumption and a wire spiral antenna, respectively, to examine the optimum relative permittivity value in the 1-6 GHz Ultrawideband (UWB) implant communications. In [27], the optimum relative permittivity of a 1 to 20 mm-thick matching layer is numerically examined by using a multilayered model (skin, fat, muscle) for different frequencies ranging from 1 GHz to 6 GHz. Similarly, in [28], the authors use a multilayered numeric model covered with an external matching layer to investigate the effect of the relative permittivity of the matching layer on the power loss reduction in the 403 MHz Medical Implant

C. Cadir, Omer A. Kati and S. Dumanli are with the Department of Electrical and Electronics Engineering, Boğaziçi University, 34343, Turkey, H. Birkan Yilmaz is with the Department of Computer Engineering, Boğaziçi University, 34343, Turkey, and E. Cil is with IETR, Université de Rennes 1, 35042, France. e-mail: sema.dumanli@boun.edu.tr. This study was supported in part by the TUBITAK 2247-A National Leader Researchers program Award No. 120C131 and the BIDEB-STAR fellowship program.

This article has been accepted for publication in a future issue of this journal, but has not been fully edited. Content may change prior to final publication. Citation information: DOI 10.1109/TAP.2022.3140497, IEEE Transactions on Antennas and Propagation

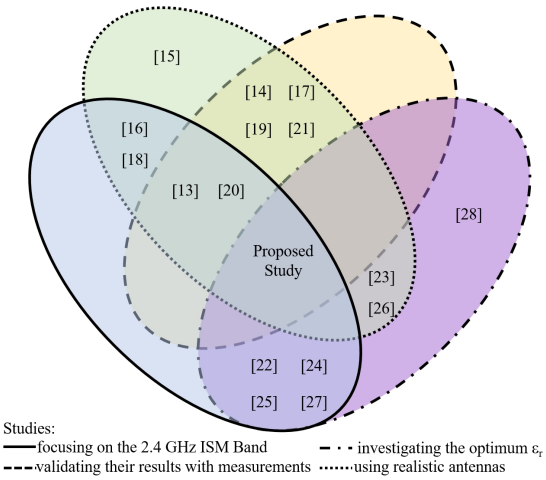

Fig. 1. The comparison of the proposed study with the related studies.

Radiocommunications Service (MedRadio) band. However, the analytical and numerical analyses performed in these studies only provide the optimum value for the specific case examined in the corresponding study. In addition, the numerical approach is computationally heavy and time-consuming, which turns the optimization for different cases into an overwhelming process.

This paper presents a novel machine learning (ML) based approach to ease the selection of the MM for different cases. Due to the rapid growth and diversity of available data, ML has become a technology that is being frequently used to find an optimized solution to a given problem in a wide variety of applications, including electromagnetics and antennas [29], [30]. ML's popularity in concepts related to electromagnetics is rooted in its ability to improve the computational cost when solving complex electromagnetic problems with a data-driven approach [31]. The studies on developing ML-based techniques for electromagnetics and antennas include but are not limited to antenna design and optimization [32]–[36], beamforming in antenna arrays [37], [38], direction of arrival estimation [39], [40], EM scattering [41], [42], and EM compatibility [43].

The novelty of this study is twofold. Firstly, over 200 cases are considered to empirically find the optimum MM permittivities for four different scenarios with three different target tissues (muscle, brain, fat) at 2.4 GHz. The impact of a well-designed MM is demonstrated for muscle and brain as target tissues with measurements. To demonstrate the gap filled with this study, a comparison of the proposed study with the studies implementing an MM in the literature in terms of four essential aspects is provided in Fig. 1. Secondly, after showing the impact of the MM in the studied cases, a more generalized ML-based tool that predicts the average Poynting vector magnitude (APVM) and the dipole length for given system parameters is proposed. The trained artificial neural network (ANN) is later used for showing the relationship between MM permittivity and APVM values. The output of the ANN was in line with the empirical results for different target tissues.

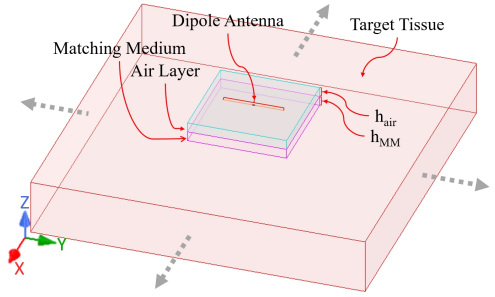

Fig. 2. The setup used to empirically determine the optimum permittivities of the MM for three different tissues (h_{MM}: MM thickness, h_{air}: air thickness).

II. The Empirical Approach

A. Data Generation with Simulations

In order to empirically find an optimum MM design for three different antenna - human body separations (1 cm, 2 cm, 3 cm) and three different target tissues (muscle, brain, fat), an extensive number of simulations are conducted with ANSYS High Frequency Structure Simulator (HFSS) [44]. The EM properties of these tissues at 2.4 GHz are tabulated in Table I [45], [46]. The simulation setup consists of a tissue-mimicking numerical phantom representing the target tissue, an MM, and an on-body wire dipole antenna, as visualized in Fig. 2. MM thicknesses of 1 cm and 2 cm are investigated. In addition, an air layer of 0 cm or 1 cm thickness is placed in between the MM and the on-body antenna, resulting in four different cases with the MM. Here, an air layer of 0 cm thickness means that the MM and on-body antenna are in contact. The conductivity of the MM is set to 0 S/m for all cases, and its relative permittivity is varied from 2 to the target tissues' relative permittivity in increments of 2, resulting in 205 different cases in total. For all 205 cases, more than 700 simulations are performed to optimize the dipole length for the operation at the 2.4 GHz resonant frequency. To eliminate the effect of an implant antenna, the simulated Poynting vectors are utilized for measuring the transmitted power levels. The APVM values are calculated inside the target tissue at depths of 4 cm, 3 cm, 2 cm, and 1 cm. The calculation is done with the HFSS fields calculator by taking the integral of the Poynting magnitudes on a rectangle surface of 1 cm × 2.5 cm and dividing by the total area. The optimum values are determined by comparing the calculated APVM values. As an example, Fig. 3 shows the APVM values as the MM permittivity changes at 4 cm depth, taking muscle as the target tissue. The APVM values change depending on the relative permittivity of the MM, resulting in a different optimum value for every different target tissue and the thickness of the MM and air layer. Finally, in order to demonstrate the effect of a well-designed MM, simulations are run for the cases where no MM is present between the tissue and the dipole antenna, that is, only an air layer of 1 cm, 2 cm or 3 cm is present between the tissue and the dipole. These 9 cases are going to be referred to as the benchmark cases.

This article has been accepted for publication in a future issue of this journal, but has not been fully edited. Content may change prior to final publication. Citation information: DOI 10.1109/TAP.2022.3140497, IEEE Transactions on Antennas and Propagation

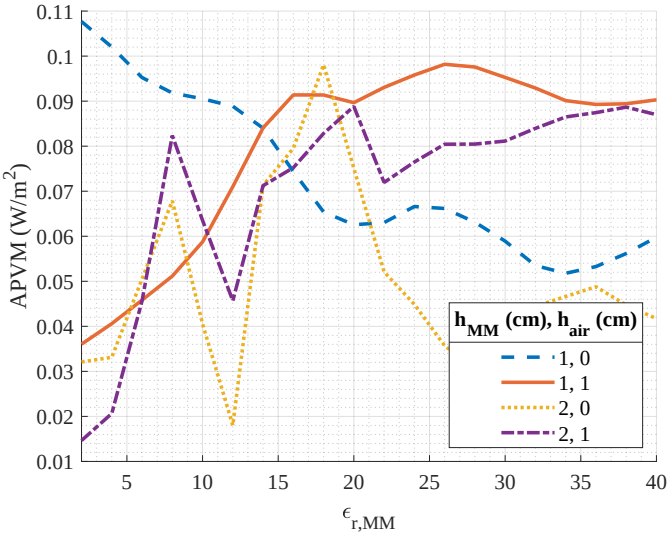

Fig. 3. Simulated (empirical) APVM at 4 cm depth with respect to the ϵ_r of the MM for different cases in the muscle tissue at 2.4 GHz.

TABLE I
EM PROPERTIES OF THE MUSCLE, BRAIN AND FAT TISSUES AT 2.4 GHZ

Tissue	Relative Permittivity	Conductivity (S/m)
Muscle	52.8	1.71
Brain	39.2	1.8
Fat	10.8	0.26

The optimum permittivities and the corresponding dipole lengths are tabulated in Table II. As mentioned before, the dipole lengths are optimized for each case. Fig. 4 presents the return loss graphs only for the optimum MM cases and the benchmark cases listed in Table II. The return loss at 2.4 GHz is greater than 10 dB for all the cases, although Fig. 4 is limited to muscle as the target tissue for the sake of conciseness. The effect of the MM on the power transmitted into the human body is evaluated by examining the Poynting vector field distributions at the corresponding depths. For instance, the Poynting vector fields plotted at 2.4 GHz and at 1 cm depth in the fat tissue for different cases studied can be seen in Fig. 5. One must note that the data used to present these Poynting vector field plots are exported in 0.5 mm steps from the simulations and then interpolated. The Poynting vectors calculated with the optimum MM are greater than their corresponding benchmark cases. The effect of the MM becomes more substantial as the separation between the antenna and the human body increases. In addition, Table II provides quantitative data supporting these arguments.

B. Validation

A setup is prepared to validate the results of the empirical search for an optimum MM detailed in Section II-A. The validation is performed through both simulations and measurements for muscle and brain as the target tissues. The setup consists of a rectangular patch antenna as the implant antenna, a dipole antenna as the on-body antenna,

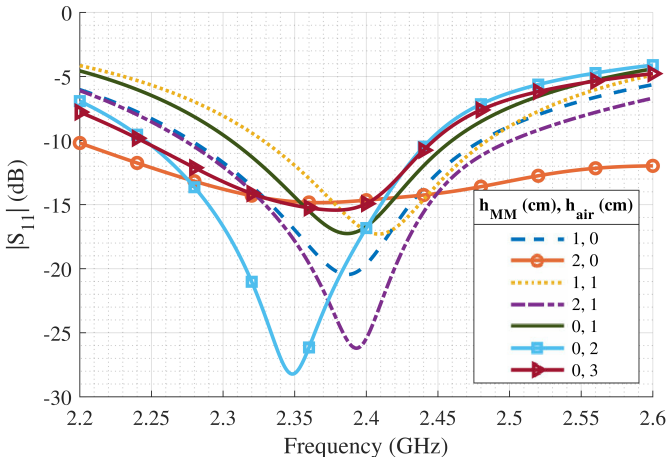

Fig. 4. Optimized $|S_{11}|$ of the dipole antenna for different cases with muscle as the target tissue.

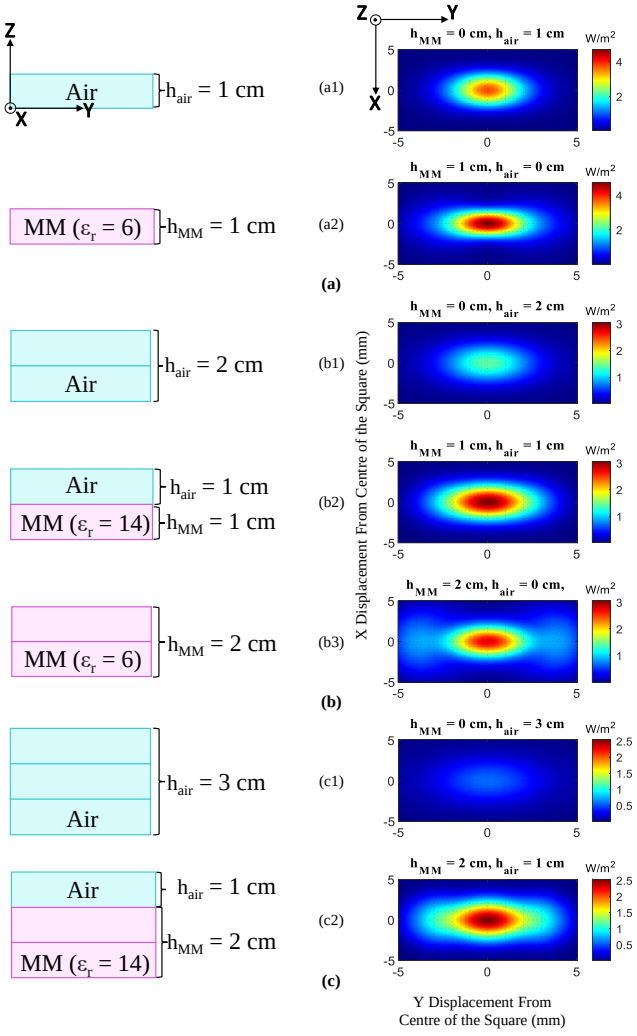

Fig. 5. Simulated Poynting vector magnitudes (W/m^2) for different cases at 1 cm depth in the fat tissue at 2.4 GHz. The figures at the left-hand side visualize the different cases studied, and the figures at the right-hand side show the corresponding Poynting vector magnitude plots on a cross-sectional area at 1 cm depth in the fat tissue for (a) 1 cm, (b) 2 cm, (c) 3 cm antenna - human body separation.

This article has been accepted for publication in a future issue of this journal, but has not been fully edited. Content may change prior to final publication. Citation information: DOI 10.1109/TAP.2022.3140497, IEEE Transactions on Antennas and Propagation

TABLE II
OPTIMUM VALUES FOR THE RELATIVE PERMITTIVITY OF THE MM, THE CORRESPONDING DIPOLE LENGTHS AND THE INTEGRALS OF THE POYNTING VECTOR MAGNITUDES COMPUTED OVER A 10 CM BY 10 CM AREA AT 4 CM, 2 CM, 1 CM DEPTHS FOR MUSCLE, BRAIN AND FAT, RESPECTIVELY

Tissue	MM Thickness (cm)	Air Thickness (cm)	Optimum MM ϵ_r	Dipole Length (mm)	Computed Integral (mW)
Muscle	1	0	2	49.9	0.18
	2		18	24.9	0.21
	1	1	26	59.9	0.2
	2		20	59.8	0.19
	0	1, 2, 3	*	59.9	0.16, 0.07, 0.04
Brain	1	0	8	32.9	0.92
	2		32	21.5	0.84
	1	1	24	60.3	0.84
	2		34	60.3	0.76
	0	1, 2, 3	*	59.9	0.67, 0.33, 0.17
Fat	1	0	6	35.9	7.13
	2		6	36.9	6.47
	1	1	14	59.9	5.81
	2		14	60.9	5.9
	0	1, 2, 3	*	59.9	5.48, 3.06, 1.77

TABLE III
AMOUNT OF EACH INGREDIENT USED FOR THE PREPARATION OF THE TISSUE-MIMICKING PHANTOMS

Ingredient	Muscle Tissue	Brain Tissue
Water (L)	3.4	2
Oil (L)	0.7	1
Dish Detergent (L)	1.2	1
Cornstarch (g)	450	400

TABLE IV
MEASURED EM PROPERTIES OF THE PREPARED TISSUE-MIMICKING PHANTOMS AND MM AT 2.4 GHZ

	Relative Permittivity	Conductivity (S/m)
Muscle Tissue	51.5	1.73
Brain Tissue	39.6	1.71
MM1	2.7	0.001
MM2	5.1	0.06
MM3	20	0.5
MM4	27	0.61
MM5	35	1.1

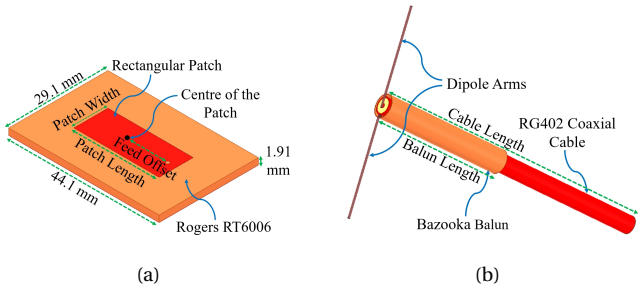

Fig. 6. The models and the parameterized dimensions of the antennas used in the simulations and the measurements. (a) the implant patch antenna. (b) the on-body dipole antenna.

a container, an elevator platform for the implant antenna, two boxes for the MM (one for 1 cm thickness and one for 2 cm thickness), tissue-mimicking phantoms and MM.

The patch antenna as seen in Fig. 6(a) is designed to operate in the 2.4 GHz Industrial, Scientific and Medical (ISM) Band on a 1.91 mm-thick Rogers RT/duroid 6006 (ϵ_r = 6.15) substrate [47]. The dimensions of the patch and the offset of the feed from the centre are 25 mm × 10 mm and 10 mm, respectively. The substrate has a size of 44.1 mm × 29.1 mm. A 1 mm spacing is introduced around the patch in order to decrease the near-field losses. The implant antenna is prototyped using LPKF S103. The dipole antenna as seen in Fig. 6(b) is designed to operate in the 2.4 GHz ISM band for 8 different cases and 6 benchmark cases. The radius of the dipoles is 0.225 mm. Each dipole is fed with a 62 mm long RG402 semi-rigid coaxial cable and a 29 mm long bazooka balun.

The container is made of plexiglass and 30 cm × 30 cm × 20 cm in size. The elevator platform and the boxes are 3D printed using polylactic acid (PLA). The tissue-mimicking phantoms and MM are prepared using the ingredients tabulated in Table III. The mixture consisting of these ingredients is continuously stirred while it is heated up to 80°C, where solidification takes place. The mixtures are then allowed to cool to room temperature. Their EM properties are measured using a Speag DAKS probe and tabulated in Table IV. As previously listed in Table II, the required MM relative permittivity values selected by the empirical approach for muscle and brain as the target tissues are 2, 18, 20, 26 and 8, 24, 32, 34, respectively. The developed MM are mapped to the required MM as follows: ϵ_r = 2 - MM1, ϵ_r = 8 - MM2, ϵ_r = 18 and ϵ_r = 20 - MM3, ϵ_r = 24 and ϵ_r = 26 - MM4, ϵ_r = 32 and ϵ_r = 34 - MM5. As can be seen in Table IV, the prepared MM have non-zero conductivity. The impact of their conductivity values is compensated for while the measurements are presented.

The bottom part of the container is filled with isotonic (0.3%) water absorbed silica to minimize EM wave penetration. The rest of the container is filled with the tissue-mimicking phantom. The implant antenna is placed on its elevator platform along with its cabling, and the surroundings of the antenna are covered with parafilm as can be seen in Fig. 7(a). The calibration is performed right before the implant antenna at the end of the coaxial cable. The elevator platform is immersed into the phantom as in Fig. 7(b). Note that the depth of the implant can be adjusted via the holes on the walls. An adjustable platform is preferred for the implant antenna, as the depth of the implant in real-life applications varies depending on in which part of the body it will be implanted. For example, a muscle implant is generally implanted deeper than a head implant. Therefore, here, it is set to 4 cm for the muscle tissue and 2 cm for the brain tissue. The box is filled with the prepared MM as shown in Fig. 7(c) and placed on top of the tissue-mimicking liquid as seen in Fig. 7(d). The final measurement setup along with the dipole antenna placed on the MM can be seen in Fig. 7(e).

Fig. 8(a) and Fig. 8(b) show the simulation and the measurement results for the transmission coefficient between the dipole and the patch antenna for the muscle tissue, respectively. The corresponding $|S_{21}|$ values at 2.4 GHz for seven different cases are tabulated in Table V. It can be

This article has been accepted for publication in a future issue of this journal, but has not been fully edited. Content may change prior to final publication. Citation information: DOI 10.1109/TAP.2022.3140497, IEEE Transactions on Antennas and Propagation

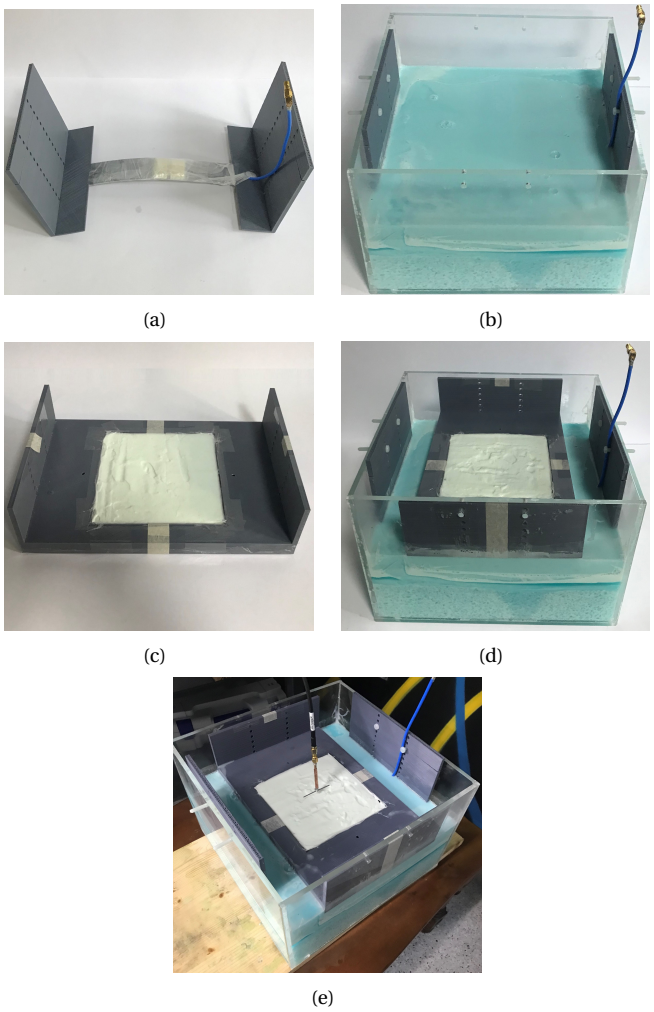

Fig. 7. The components and the preparation of the measurement setup. (a) The implant antenna placed on the elevator platform covered with parafilm. (b) The elevator platform placed inside the container. (c) The box filled with the MM. (d) The box placed on the tissue-mimicking phantom. (e) The complete measurement setup with the dipole antenna.

observed that the MM does not improve the $|S_{21}|$ values for 1 cm separation between the on-body antenna and the human body. However, when the separation is increased, the effect of the MM becomes substantial. For instance, for 2 cm separation, it can be seen that MM increases the $|S_{21}|$ value at 2.4 GHz from approximately -30 dB to approximately -25 dB. Similarly, for 3 cm separation, MM improves the $|S_{21}|$ value by approximately 8 dB. Note that the measured values are corrected to compensate for the non-zero conductivity values of the developed MM. For this correction, each measurement case including an MM is simulated first with the non-conductive MM and next with the corresponding conductive MM. The difference between the simulated $|S_{21}|$ values are added to the measured values.

Fig. 8(c) and Fig. 8(d) show the simulation and the measurement results for the brain tissue, respectively. The corresponding $|S_{21}|$ values at 2.4 GHz are tabulated in Table V. As can be seen, the $|S_{21}|$ value is increased from approximately -22 dB to approximately -18 dB for 2 cm separation and the improvement in the $|S_{21}|$ value is approximately 8 dB for 3 cm separation. The improvement in the measured 2 cm thick MM case is lower than the estimated one for the brain tissue due to the direct contact between the on-body antenna and the conductive MM that leads to high near-field losses. Note that the conductivity of the MM developed for that case is particularly higher due to its high water content. In an ideal setup, an MM with no conductivity would be used, eliminating this problem.

TABLE V
SIMULATED AND CORRECTED MEASURED $|S_{21}|$ VALUES FOR DIFFERENT CASES FOR THE MUSCLE TISSUE AND THE BRAIN TISSUE AT 2.4 GHZ

	Tissue			
	Muscle		Brain	
h_{MM}, h_{air} (cm), (cm)	Simul. $\|S_{21}\|$ (dB)	Corrected Meas. $\|S_{21}\|$ (dB)	Simul. $\|S_{21}\|$ (dB)	Corrected Meas. $\|S_{21}\|$ (dB)
0, 1	-24.3	-24.4	-16.7	-16.3
1, 0	-24.7	-25.2	-18.1	-17.9
0, 2	-29.8	-30.3	-22.3	-22
1, 1	-24.5	-24.4	-17.2	-16.7
2, 0	-25.2	-27	-19.6	-21.8
0, 3	-33.8	-34	-26.6	-26.1
2, 1	-25.1	-25	-18	-17.2

TABLE VI
INTEGRALS OF THE POYNTING VECTOR MAGNITUDES COMPUTED OVER A 1.5 CM BY 2.5 CM AREA AND THE SIMULATED $|S_{21}|$ VALUES FOR THE SINGLE LAYER AND THE REALISTIC HUMAN HEAD MODEL

	Computed Integral (mW)	$\|S_{21}\|$ (dB)
Single-layer	0.15	-47.6
Realistic	0.14	-45.2

It can be noticed that this work uses single-layer tissue models as target tissues, whereas the human body consists of layers of different tissues in real life. Hence, one may ask whether the results obtained in this work can be extended to a multi-tissue realistic human body model. In order to investigate this, two simulation setups are prepared. The first setup includes a homogeneous single-layer head model, whereas the second setup includes an ANSYS human head phantom model (Male-4 mm accuracy) with different tissues. The implant antenna is placed at 4 cm depth. The case with 2 cm thick MM and 0 cm thick air layer is selected for this investigation. The results are tabulated in Table VI. It can be seen that the $|S_{21}|$ and the computed integral values agree very well for the two different head models. Hence, the results of the single-layer tissue models can be extended to multi-tissue realistic models. Moreover, a single-layer model may be preferable during the design as it decreases the simulation time without significantly affecting the accuracy.

III. THE MACHINE LEARNING-BASED APPROACH

The ML-based approach studied in this work aims to determine the optimum MM permittivity by considering the properties of the target tissues together with the desired MM and air layer thicknesses. For this purpose, an ANN

This article has been accepted for publication in a future issue of this journal, but has not been fully edited. Content may change prior to final publication. Citation information: DOI 10.1109/TAP.2022.3140497, IEEE Transactions on Antennas and Propagation

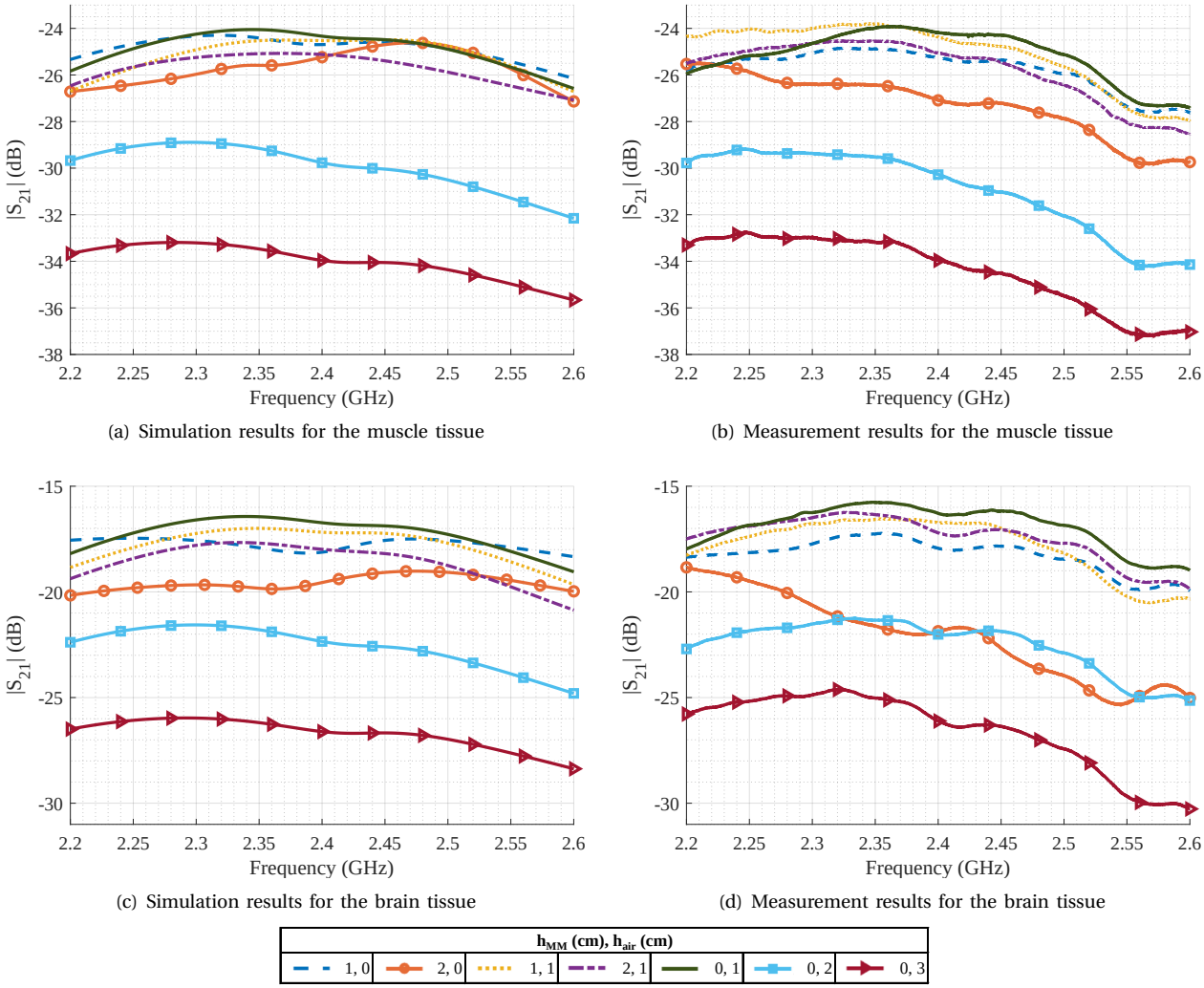

(a) Simulation results for the muscle tissue

(b) Measurement results for the muscle tissue

(c) Simulation results for the brain tissue

(d) Measurement results for the brain tissue

Fig. 8. Simulated and corrected measured $|S_{21}|$ between the implant antenna and the on-body antenna for different cases.

model that predicts the dipole length and the AVPM for a given setting is proposed. This proposed ANN model is remarkably fast compared to the simulations, allowing one to predict the dipole length and the AVPM in the order of milliseconds. After obtaining a number of predictions by sweeping different MM permittivities, the case with the highest AVPM is selected as the optimum case. The associated MM permittivity is determined as the optimum for the specified setting. The proposed ANN model consists of a one-dimensional convolutional neural network (CNN) and fully connected (FC) layers.

This section consists of four parts. First, the generation of the data set and the data representation are explained. Next, the ANN structure is demonstrated, and the experiment details and results are given.

A. Data Set

As previously mentioned in Subsection II-A, a total of 205 cases that differ from each other in MM thickness, air layer thickness, target tissue type, and MM relative permittivity are examined during the empirical approach. For the ML-based approach, the simulation results obtained in the empirical approach are used as the data set. From these 205 different cases, randomly selected cases with muscle (25 cases) and brain tissues (20 cases) are split as the test set. The remaining cases with muscle (73 cases), brain (59 cases), and fat tissues (28 cases) are employed for training and validation purposes in a 5-fold cross-validation scheme.

Each data sample (case) is represented with a two-channel one-dimensional image slice and three numerical inputs for defining the setup. The first channel of the image slice denotes the relative permittivity, whereas the second one denotes the conductivity. The image slice is a vertical cut of the system from the on-body antenna to the implant surface, where pixels represent layers with equal thicknesses, as illustrated in Fig. 9(a). The input dimension is fixed to 210 so that the resolution is high enough to get only a single pair of EM properties corresponding to a single pixel for all considered depths and MM thicknesses. The physical distance between the on-body antenna and the implant surface is not constant for all cases due to the varying thicknesses of the MM and the air layer. Thus, the physical thickness of a pixel depends on the data sample

This article has been accepted for publication in a future issue of this journal, but has not been fully edited. Content may change prior to final publication. Citation information: DOI 10.1109/TAP.2022.3140497, IEEE Transactions on Antennas and Propagation

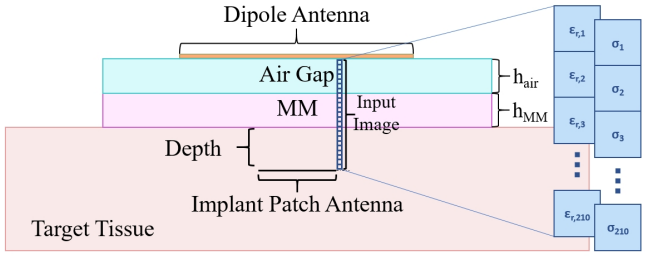

(a) Physical illustration of the input image slice.

(b) The overall structure.

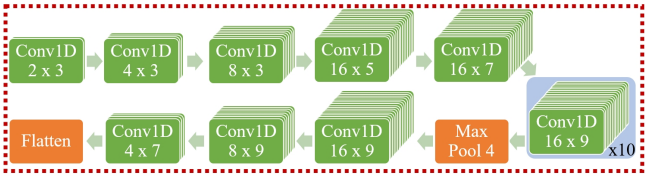

(c) The CNN structure.

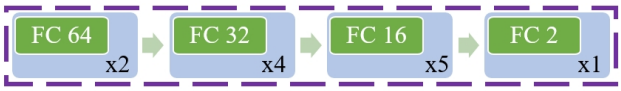

(d) The MLP structure.

Fig. 9. The artificial neural network structure.

TABLE VII
INPUTS AND OUTPUTS OF THE NEURAL NETWORK

Inputs	Vertical Cut Image Slice 210×2
	Resonant Frequency
	Depth of the Implant Antenna
	Stepsize of the Input Image Slice
Outputs	APVM
	Electrical Length of the Dipole

and is fed as a numerical input in units of millimeters. Other numerical inputs mark the deviation of the resonant frequency from 2.4 GHz in units of GHz and the depth of the implant antenna in centimeters. The channels of the input are normalized by dividing each channel with the explicit limits for the relative permittivity and the conductivity of the human body tissues [45], [46], which are 82.41 and 3.41 S/m, respectively. The outputs are the APVM value and the electrical length of the dipole. Both outputs are scaled to the (0, 1) range before training for faster convergence. The inputs and outputs are summarized in Table VII.

B. Proposed ANN Model

The proposed ANN structure is depicted in Fig. 9. It starts with two branches, a CNN and FC layer, which are then joined and followed by a multi-layer perceptron (MLP) (Fig. 9(b)). CNN is used to process the input image slice, and the FC layer aims to equate the dimension of the numerical inputs to the dimension of the CNN outputs.

The CNN (Fig. 9(c)) part of the model consists of one-dimensional convolutional layers of varying kernel width with up to 16 filters and a maximum pooling layer of kernel width 4. The flattened CNN outputs are concatenated with the FC layer outputs and fed into MLP. The MLP (Fig. 9(d)) part has 6 FC layers consisting of 2, 16, 32, and 64 neurons, For all layers, ReLU activation is used.

C. ANN Experiments

Experiments are carried out by implementing the proposed ANN model with Keras library [48] and using the data set derived from simulation output for various cases of brain, muscle, and fat tissues. Adam optimizer with learning rate 0.001 and mean square error (MSE) loss is utilized. Moreover, mean absolute error (MAE) and mean absolute percentage error (MAPE) are monitored.

The network is trained with a batch size of 32 for 3000 epochs. Excluding the test set samples, 5-fold cross-validation is employed on the data set. The model with the best performance is determined by monitoring MSE, MAE, and MAPE on the validation set. This model is trained on the dataset using all 5 folds for 3000 epochs to achieve the final trained model.

D. Results

The proposed ANN structure is chosen carefully by inspecting the joint errors of the dipole length and the AVPM on the training and validation sets, which is the usual way of proposing an ANN model. A model with an ideal structure should learn the cases in the training set and generalize well, i.e., predict the cases in the validation set with low error. To illustrate that the proposed model conforms to these goals compared to the similar models, three 5-fold cross-validation experiments are run by changing the number of filters (for CNN) and neurons (for FC). The number of filters and neurons is increased with a factor of 1.5 and 2 to yield two model structures of higher complexity. Then, the number of filters and neurons is halved to get a lower-complexity model. These three models and the proposed model are trained using a 5-fold cross-validation scheme. The results of these experiments are reported in Table VIII. As can be seen, the training and validation errors of the model with the lowest complexity cannot reach the level of the proposed model, suggesting that its' expressive power is not enough. The model with the highest complexity cannot converge to learn the cases in the training set. Also, the training time increases with the complexity of the model. Thus, the proposed model matches the desired complexity level while achieving a satisfactory estimation performance.

The average and best case errors for the 5-fold cross-validation is given in Table IX and Table X. The best case is selected with respect to the smallest MAPE on the validation set for the APVM since the results indicate that this output is harder to estimate compared to the other one. To make the best use of the available data set, the selected ANN

This article has been accepted for publication in a future issue of this journal, but has not been fully edited. Content may change prior to final publication. Citation information: DOI 10.1109/TAP.2022.3140497, IEEE Transactions on Antennas and Propagation

TABLE VIII
MSE, MAE AND MAPE FOR JOINT DIPOLE LENGTH [mm] AND APVM [W/m^2] ON THE TRAINING AND VALIDATION SETS FOR 5-FOLD CROSS VALIDATION OF THREE STRUCTURES WITH HALF, ORIGINAL, AND DOUBLE NUMBER OF FILTERS

Set	ANN Structure	MSE	MAE	MAPE
Train	Half	0.000194	0.007116	1.248411
	Original	0.000041	0.004128	0.716885
	One and a Half	0.000288	0.008006	1.436288
	Double	0.290524	0.380760	50.421369
Valid	Half	0.001120	0.015322	2.736528
	Original	0.000849	0.013065	2.343896
	One and a Half	0.002000	0.018200	3.238683
	Double	0.290510	0.380752	50.423455

TABLE IX
MSE, MAE AND MAPE FOR APVM [W/m^2] ON THE TRAINING AND VALIDATION SETS FOR 5-FOLD CROSS VALIDATION

Set	Case	MSE	MAE	MAPE
Train	Average	0.435003	0.276674	45.53026
	Best	0.000215	0.010768	7.649216
Valid	Average	0.435753	0.310152	53.73685
	Best	0.025948	0.06674	16.71386
Train (5 folds)		0.002623	0.024548	12.68722

model is used as the initial point and it is trained on all 5-folds of the data set, and the resulting training errors are reported in Table IX and Table X.

By employing the trained model on the test set, the errors are calculated for individual samples. Then, 10% of the test samples with the highest and lowest absolute percentage error (5% each) in APVM estimation are trimmed. In Fig. 10, the ANN estimations of APVM and dipole length are compared with the empirical values. In Fig. 10(a), it is observed that the deviations of APVM estimations from the empirical values are limited, and there are only a few significant deviations. As seen in Fig. 10(b), the dipole length estimations are nearly perfect.

In the test set, the resulting mean errors are given in Table XI and Table XII. It is observed that lower APVM values are more likely to be estimated with a higher percentage error. The reason is the scarcity of training data samples having low APVM. Our model can predict the APVM greater than 0.25 W/m^2 with 12.3% MAPE and the dipole length with 1% MAPE over all cases.

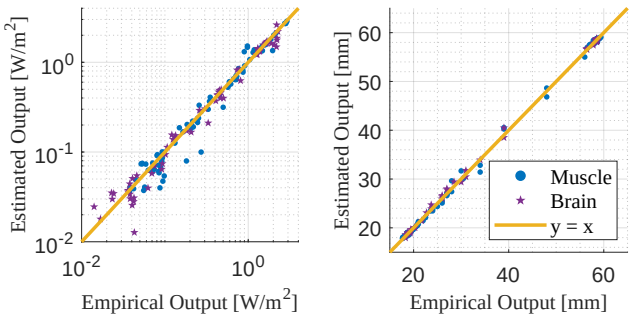

(a) APVM estimation (b) Dipole length estimation

Fig. 10. The comparison of empirical and estimated outputs (ANN).

TABLE X
MSE, MAE AND MAPE FOR THE DIPOLE LENGTH [mm] ON THE TRAINING AND VALIDATION SETS FOR 5-FOLD CROSS VALIDATION

Set	Case	MSE	MAE	MAPE
Train	Average	0.038217	0.144298	0.443574
	Best	0.032637	0.139636	0.412054
Valid	Average	0.306984	0.290243	0.879405
	Best	0.650546	0.45318	1.364362
Train (5 folds)		0.064463	0.191067	0.590357

TABLE XI
MSE, MAE AND MAPE FOR APVM [W/m^2] ON THE TEST SET

Tissue	APVM [W/m^2]	MSE	MAE	MAPE
Muscle	All	0.014478	0.057418	13.83549
	<0.25	0.000574	0.016261	16.63462
	>0.25	0.027802	0.096861	11.15298
Brain	All	0.020684	0.06621	16.78219
	<0.25	7.37E-05	0.007368	47.67077
	>0.25	0.023049	0.072962	13.2376
All	All	0.017083	0.061109	15.07237
	<0.25	0.000508	0.015086	20.73374
	>0.25	0.025142	0.083486	12.3196

One of the goals of this study is to find the relative permittivity value that gives the maximum APVM value for different cases. The ANN estimations are generally able to reflect the relationship between the MM permittivity and APVM. As an example, three cases for different tissues are given in Fig. 11 showing the APVM values corresponding to selected MM permittivity. The general trend is in line with the empirical data for most cases. The peaks of the empirical and estimated APVM are nearly at the same MM permittivity values for all cases in Fig. 11. The AVPM value itself does not play an important role when choosing the optimum MM permittivity, and instead where the peaks occur is of interest. Thus, the ANN approach is promising, and its limitations can be overcome by increasing the size of the data set.

IV. CONCLUSION

In this paper, over 200 cases are considered in order to empirically determine the optimum MM permittivity values at 2.4 GHz for four different scenarios and three different target tissues (muscle, brain, fat). The effect of a well-designed MM on the power transmitted into the human body is demonstrated for muscle and brain tissues through measurements. It is shown that the $|S_{21}|$ values can be enhanced up to 8 dB with the introduction of the MM. Next, a more generalized ML-based tool for the selection of the optimum MM is presented. A one-dimensional convolutional neural network followed by a

TABLE XII
MSE, MAE AND MAPE FOR THE DIPOLE LENGTH [mm] ON THE TEST SET

Tissue	MSE	MAE	MAPE
Muscle	0.296405	0.359924	1.126493
Brain	0.143705	0.250347	0.79608
All	0.232308	0.313928	0.987801

This article has been accepted for publication in a future issue of this journal, but has not been fully edited. Content may change prior to final publication. Citation information: DOI 10.1109/TAP.2022.3140497, IEEE Transactions on Antennas and Propagation

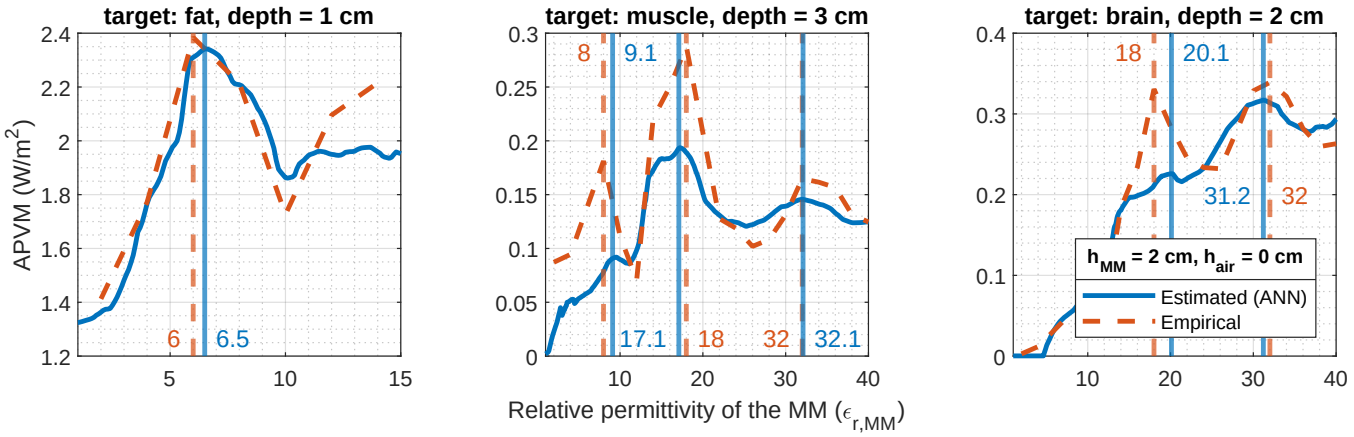

Fig. 11. Simulated (empirical) and estimated (ANN) APVM with respect to the relative permittivity of the MM for different cases. The vertical lines show where the peaks occur, which leads to finding the optimum MM permittivity.

multi-layer perceptron is trained with the simulated APVM and dipole length values. The developed tool can predict the dipole length and APVM values greater than 0.25 W/m^2 with 1% and 12.3% MAPE, respectively. ANN estimator can show the relationship between MM permittivity and APVM by changing the input MM permittivity. A good coherence is observed between MM permittivity and APVM values from ANN output with minor deviations for different target tissues. Since the inputs of the ANN are flexible, the ANN estimator can be extended to accommodate layered MM and target tissues. As a future direction, we plan to increase the size of the data set to improve the ANN performance and better generalization.

ACKNOWLEDGMENT

The authors would like to give special thanks to Burak Ferhat Ozcan and Fatih Dogangun for their valuable support during the measurements.

REFERENCES

[1] A. Valanarasi and R. Dhanasekaran, "A review on design considerations of implantable antennas," in *Int. Conf. on Advanced Communication Control and Computing Technologies (ICACCCT)*, pp. 207–211, 2016.

[2] T. Karacolak, A. Z. Hood, and E. Topsakal, "Design of a dual-band implantable antenna and development of skin mimicking gels for continuous glucose monitoring," *IEEE Tran. Microwave Theory and Techniques*, vol. 56, no. 4, pp. 1001–1008, 2008.

[3] Y. Liu, Y. Chen, H. Lin, and F. H. Juwono, "A novel differentially fed compact dual-band implantable antenna for biotelemetry applications," *IEEE Antennas and Wireless Propagation Letters*, vol. 15, pp. 1791–1794, 2016.

[4] Y. Yi, J. Chen, M. Selvaraj, Y. Hsiang, and K. Takahata, "Wireless hyperthermia stent system for restenosis treatment and testing with swine model," *IEEE Trans. Biomedical Eng.*, vol. 67, no. 4, pp. 1097–1104, 2020.

[5] T. Z. Wong, J. W. Strohbehn, K. M. Jones, J. A. Mechling, and B. S. Trembly, "SAR patterns from an interstitial microwave antenna-array hyperthermia system," *IEEE Trans. Microwave Theory and Techniques*, vol. 34, no. 5, pp. 560–567, 1986.

[6] A. Kiourti and K. S. Nikita, "A review of implantable patch antennas for biomedical telemetry: Challenges and solutions [wireless corner]," *IEEE Antennas and Propagation Magazine*, vol. 54, no. 3, pp. 210–228, 2012.

[7] A. W. Damaj, H. M. El Misilmani, and S. A. Chahine, "Implantable antennas for biomedical applications: An overview on alternative antenna design methods and challenges," in *Int. Conf. on High Performance Computing Simulation (HPCS)*, pp. 31–37, 2018.

[8] T. Dissanayake, K. P. Esselle, and M. R. Yuce, "Dielectric loaded impedance matching for wideband implanted antennas," *IEEE Trans. Microwave Theory and Techniques*, vol. 57, no. 10, pp. 2480–2487, 2009.

[9] A. K. Skrivervik, "Implantable antennas: The challenge of efficiency," in *European Conf. on Antennas and Propagation (EuCAP)*, pp. 3627–3631, 2013.

[10] H. Lui, A. Fhager, and M. Persson, "Matching medium for biomedical microwave imaging," in *Int. Symp. on Antennas and Propagation (ISAP)*, pp. 1–3, 2015.

[11] O. Habiboglu, S. Akgun, E. Cil, O. A. Civi, and S. Dumanli, "Additive manufactured matching medium design for implant communications," in *European Conf. on Antennas and Propagation (EuCAP)*, pp. 1–5, 2021.

[12] C. Cadir, O. A. Kati, and S. Dumanli, "Matching medium design for in-body communications using artificial neural networks," in *European Conf. on Antennas and Propagation (EuCAP)*, pp. 1–5, 2021.

[13] G. A. Conway and W. G. Scanlon, "Antennas for over-body-surface communication at 2.45 ghz," *IEEE Trans. Antennas and Propagation*, vol. 57, no. 4, pp. 844–855, 2009.

[14] W. C. Choi, S. Lim, and Y. J. Yoon, "Design of noninvasive hyperthermia system using transmit-array lens antenna configuration," *IEEE Antennas and Wireless Propagation Letters*, vol. 15, pp. 857–860, 2016.

[15] P. Stauffer, F. Rossetto, M. Leencini, and G. Gentilli, "Radiation patterns of dual concentric conductor microstrip antennas for superficial hyperthermia," *IEEE Trans. Biomedical Eng.*, vol. 45, no. 5, pp. 605–613, 1998.

[16] S. Singh, B. Sahu, and S. P. Singh, "Hyperthermia performance of conformal applicator for limb tumor in presence of water bolus," in *Int. Symp. on Antennas and Propagation (ISAP)*, pp. 1–2, 2017.

[17] E. Porter, A. Santorelli, M. Coates, and M. Popović, "Microwave breast imaging: Time-domain experiments on tissue phantoms," in *IEEE Int. Symp. on Antennas and Propagation (APSURSI)*, pp. 695–698, 2011.

[18] S. Mahajan, A. Mane, and B. Naik, "Modelling of sleeve monopole antenna in a coupling medium for breast imaging application," in *IEEE Distributed Computing, VLSI, Electrical Circuits and Robotics (DISCOVER)*, pp. 252–254, 2016.

[19] T. Dissanayake, K. P. Esselle, and M. Yuce, "UWB antenna impedance matching in biomedical implants," in *European Conf. on Antennas and Propagation*, pp. 3523–3526, 2009.

[20] L.-J. Xu, Y.-X. Guo, and W. Wu, "Miniaturized dual-band antenna for implantable wireless communications," *IEEE Antennas and Wireless Propagation Letters*, vol. 13, pp. 1160–1163, 2014.

[21] I. Munina, P. Turalchuk, E. Kunakovskaya, and I. Vendik, "Attenuation of electromagnetic waves radiated by an implanted antenna," in *Days on Diffraction (DD)*, pp. 309–313, 2016.

[22] C. Rappaport, "Determination of bolus dielectric constant for opti-

mum coupling of microwaves through skin for breast cancer imaging," *Int. Journal of Antennas and Propagation*, vol. 2008, 03 2008.
[23] M. Wang, L. Crocco, and M. Cavagnaro, "On the design of a microwave imaging system to monitor thermal ablation of liver tumors," *IEEE Journal of Electromagnetics, RF and Microwaves in Medicine and Biology*, pp. 1–1, 2021.
[24] H.-S. Lui and A. Fhager, "On the matching medium for microwave-based medical diagnosis," *Biomedical Physics & Eng. Express*, vol. 4, p. 035015, mar 2018.
[25] R. Chávez-Santiago, A. Khaleghi, and I. Balasingham, "Matching layer for path loss reduction in ultra wideband implant communications," *Int. Conf. of the IEEE Eng. in Medicine and Biology Society (EMBC)*, vol. 2014, pp. 6989–92, 08 2014.
[26] A. Khaleghi, I. Balasingham, and R. Chávez-Santiago, "An ultra-wideband wire spiral antenna for in-body communications using different material matching layers," *Int. Conf. of the IEEE Eng. in Medicine and Biology Society (EMBC)*, vol. 2014, pp. 6985–8, 08 2014.
[27] S. Genovesi, I. R. Butterworth, J. E. C. Serrallés, and L. Daniel, "Metasurface matching layers for enhanced electric field penetration into the human body," *IEEE Access*, vol. 8, pp. 197745–197756, 2020.
[28] F. Merli, B. Fuchs, J. R. Mosig, and A. K. Skrivervik, "The effect of insulating layers on the performance of implanted antennas," *IEEE Trans. Antennas and Propagation*, vol. 59, no. 1, pp. 21–31, 2011.
[29] H. M. E. Misilmani and T. Naous, "Machine learning in antenna design: An overview on machine learning concept and algorithms," in *Int. Conf. on High Performance Computing Simulation (HPCS)*, pp. 600–607, 2019.
[30] C. Maeurer, P. Futter, and G. Gampala, "Antenna design exploration and optimization using machine learning," in *European Conf. on Antennas and Propagation (EuCAP)*, pp. 1–5, 2020.
[31] A. Massa, D. Marcantonio, X. Chen, M. Li, and M. Salucci, "Dnns as applied to electromagnetics, antennas, and propagation—a review," *IEEE Antennas and Wireless Propagation Letters*, vol. 18, no. 11, pp. 2225–2229, 2019.
[32] K. Siakavara, "Artificial neural network employment in the design of multilayered microstrip antenna with specified frequency operation," *Piers Online*, vol. 3, pp. 1278–1282, 01 2007.
[33] B. Liu, H. Aliakbarian, Z. Ma, G. A. E. Vandenbosch, G. Gielen, and P. Excell, "An efficient method for antenna design optimization based on evolutionary computation and machine learning techniques," *IEEE Trans. Antennas and Propagation*, vol. 62, no. 1, pp. 7–18, 2014.
[34] J. Tak, A. Kantemur, Y. Sharma, and H. Xin, "A 3-d-printed w-band slotted waveguide array antenna optimized using machine learning," *IEEE Antennas and Wireless Propagation Letters*, vol. 17, no. 11, pp. 2008–2012, 2018.
[35] Y. Sharma, H. H. Zhang, and H. Xin, "Machine learning techniques for optimizing design of double t-shaped monopole antenna," *IEEE Trans. Antennas and Propagation*, vol. 68, no. 7, pp. 5658–5663, 2020.
[36] Jain, "Bandwidth enhancement of patch antennas using neural network dependent modified optimizer," *Int. Journal of Microwave and Wireless Technologies*, vol. 8, pp. 1–9, 04 2015.
[37] A. Zooghby, C. Christodoulou, and M. Georgiopoulos, "Neural network-based adaptive beamforming for one- and two-dimensional antenna arrays," *IEEE Trans. Antennas and Propagation*, vol. 46, no. 12, pp. 1891–1893, 1998.
[38] P.-R. Chang, W.-H. Yang, and K.-K. Chan, "A neural network approach to MVDR beamforming problem," *IEEE Trans. Antennas and Propagation*, vol. 40, no. 3, pp. 313–322, 1992.
[39] Z.-M. Liu, C. Zhang, and P. S. Yu, "Direction-of-arrival estimation based on deep neural networks with robustness to array imperfections," *IEEE Trans. Antennas and Propagation*, vol. 66, no. 12, pp. 7315–7327, 2018.
[40] K. A. Gotsis, K. Siakavara, and J. N. Sahalos, "On the direction of arrival (doa) estimation for a switched-beam antenna system using neural networks," *IEEE Trans. Antennas and Propagation*, vol. 57, no. 5, pp. 1399–1411, 2009.
[41] H. M. Yao, L. Jiang, and W. E. I. Sha, "Enhanced deep learning approach based on the deep convolutional encoder–decoder architecture for electromagnetic inverse scattering problems," *IEEE Antennas and Wireless Propagation Letters*, vol. 19, no. 7, pp. 1211–1215, 2020.
[42] Z. Wei and X. Chen, "Deep-learning schemes for full-wave nonlinear inverse scattering problems," *IEEE Trans. Geoscience and Remote Sensing*, vol. 57, no. 4, pp. 1849–1860, 2019.
[43] L. Jiang, H. Yao, H. Zhang, and Y. Qin, "Machine learning based computational electromagnetic analysis for electromagnetic compatibility," in *2018 IEEE Int. Conf. on Computational Electromagnetics (ICCEM)*, pp. 1–2, 2018.
[44] "Ansys HFSS." http://www.ansys.com/products/electronics/ansys-hfss, May 2021.
[45] "IT'IS Foundation Dielectric Properties Database." https://itis.swiss/virtual-population/tissue-properties/database/dielectric-properties/, May 2021.
[46] R. E. Fields, "Evaluating compliance with FCC guidelines for human exposure to radiofrequency electromagnetic fields," *OET bulletin*, vol. 65, no. 10, 1997.
[47] K. Godeneli, U. Bengi, O. A. Kati, and S. Dumanli, "A wearable repeater antenna for implant communications," *IEEE Trans. Antennas and Propagation*, 2021, accepted.
[48] F. Chollet *et al.*, "Keras." https://keras.io, 2015.

Erdem Cil received the Bachelors degree in electronics and communication engineering from Istanbul Technical University, Istanbul, Turkey, in 2017 and the Masters degree from Boğaziçi University, Istanbul, Turkey, in 2020. He was also a Research Assistant with the Electronics Department, Boğaziçi University.

He is currently pursuing the PhD degree with IETR, University of Rennes 1, Rennes, France. His current research interests include ingestible and implantable antenna design.

Cemre Cadir is currently studying electrical and electronics engineering at Boğaziçi University, Istanbul, Turkey. She was an erasmus student at Technical University of Denmark, Denmark in Fall 2019.

She was a member of the Antennas & Propagation Research Laboratory (BOUNtenna) from 2018 to 2021. Her current research interests include communications and machine learning.

Omer A. Kati is currently studying electrical and electronics engineering at Boğaziçi University, Istanbul, Turkey. He was an erasmus student at Poznan University of Technology, Poland in Spring 2021.

He is currently a member of the Antennas & Propagation Research Laboratory (BOUNtenna). His current research interests include machine learning and its applications in wearable antenna design and implant communications.

H. Birkan Yilmaz (S'10-M'12) received the B.S. degree in mathematics, and the M.Sc. and Ph.D. degrees in computer engineering from Boğaziçi University, Istanbul, Turkey, in 2002, 2006, and 2012, respectively.

He worked as a Post-Doctoral Researcher with the Yonsei Institute of Convergence Technology, Yonsei University, South Korea, for four years, and with the Universitat Politecnica de Catalunya, Spain, for two years. He is currently an Assistant Professor with the Department of Computer Engineering, Boğaziçi University, Istanbul, Turkey. His research interests include cognitive radio, spectrum sensing, molecular communications, and multiscale communications.

Sema Dumanli (M'11) received the Bachelors degree in electrical and electronic engineering from Orta Doğu Teknik Üniversitesi, Ankara, Turkey, in 2006 and the Ph.D. degree from the University of Bristol, Bristol, U.K., in 2010.

She was with Toshiba Research Europe, Bristol, as a Research Engineer and a Senior Research Engineer from 2010 to 2017. She is currently an Assistant Professor with Boğaziçi University, Istanbul, Turkey. Her current research interests include antenna design for body area networks, implantable and wearable devices, eHealth, and multiscale communications.